DOI: 10.1002/ejic.200600488

# Identification of the Dinuclear and Tetranuclear Air-Oxidized Products Derived from Labile Phenolate-Bridged Dimanganese(II) Pyridyl-Chelate Compounds

**Frank Bartnik Larsen,[a] Astrid Boisen,[a] Kevin J. Berry,[b] Boujemaa Moubaraki,[c] Keith S. Murray,[c] Vickie McKee,[d] Robert C. Scarrow,[e] and Christine J. McKenzie*[a]**

**Keywords:** Manganese / O ligands / Chelates / Bond valence sum analysis / Oxidation

Dioxygen-sensitive dinuclear manganese complexes of the phenoxo-hinged dinucleating ligand 2,6-bis{[*N*,*N*′-bis(2-picolyl)amino]methyl}-4-*tert*-butylphenolato (bpbp$^-$) containing exogenous labile THF, water and perchlorato ligands are described. The manganese(II) complexes $[Mn_2(bpbp)(ClO_4)_2(THF)]^+$ (**1**) and $[Mn_2(bpbp)(ClO_4)(H_2O)_2]^{2+}$ (**2**) have been isolated as the salts **1**·$ClO_4$·THF·$3H_2O$, **1**·$B(C_6H_5)_4$·4THF and **2**·$(ClO_4)_2$·$H_2O$. Complexes **1** and **2** are spontaneously oxidised in air in solution and the solid state. The reaction products of the air oxidation in THF, water and methanol solutions are labile dinuclear $Mn^{II}$–$Mn^{III}$, $Mn^{III}_2$ and $Mn^{III}$–$Mn^{IV}$ complexes containing water- and methanol-derived exogenous ligands. In addition, a $Mn_4$ complex has been isolated. Magnetic susceptibility data confirm the $Mn^{II}$–$Mn^{III}$ oxidation state assignment with an $S = 2/S = 5/2$ model with weak antiferromagnetic coupling ($J = -3.7$ cm$^{-1}$) in $[Mn_2(bpbp)(CH_3O)_2(H_2O)_2](ClO_4)_2$ [**3**·$(ClO_4)_2$]. A tetranuclear complex, $[Mn_4(O)_{4-n}(OH)_n(bpbp)_2](ClO_4)_4$ [$n$ = 1 or 2; **7**·$(ClO_4)_4$], recovered from THF shows a $Mn_4O_6$ adamantane-type core with the O bridges furnished by the two phenolato groups and four hydroxide/oxide bridges. We have arrived at two feasible formulations for the core metal oxidation states and oxo-bridge protonation states, namely $[Mn^{III}_4(O)_2(OH)_2(bpbp)_2]^{4+}$ and $[Mn^{III}_3Mn^{IV}(O)_3(OH)(bpbp)_2]^{4+}$, for **7**, on the basis of a bond valence sum analysis of the crystal structure, elemental analysis and XANES. Thus, complex **7** is at least two oxidation state levels lower than known complexes with the $Mn_4O_6$ adamantane core structure. The magnetism of **7** was fitted well to an $Mn^{III}_4$ three-*J* model. Complex cations related to **3** by homology, and to **7** by hydration/solvation, have been identified by ESI mass spectrometry. The $[Mn_2(bpbp)(OH)_2(H_2O)_2]^{2+}$ ion (**4**) present in aqueous solutions on dissolution of **1**·$ClO_4$·THF·$3H_2O$ in air or by simple dissolution of **3** in water-containing solvent is isoelectronic to **3**. In the presence of significant amounts of water the $Mn^{II}$–$Mn^{III}$ complexes **3** and **4** are susceptible to further metal oxidation and concomitant aquo ligand deprotonation to give ions assignable to $[Mn^{III/IV}_2(bpbp)O(OCH_3)_2(H_2O)]^{2+}$ (**5**) and $[Mn^{III}_2(bpbp)(OH)_3(H_2O)]^{2+}$ (**6**). ESI mass spectra of water or methanol solutions of **1**, **2**, **3** and **7** show predominantly an ion assignable to the oxide $[Mn_2(bpbp)(O)]^{2+}$ (**8**). Cation **8** is most likely not present in solution. Using mild source conditions and MS-MS techniques, the gas-phase fragmentation pathways to generate **8** have been mapped.


## Introduction

Dinuclear manganese compounds are of considerable interest due to their potential as catalysts for oxidation reactions in which hydrogen peroxide or, better, dioxygen are used as the terminal oxidant.[1] We have discovered that a dimanganese complex of the dinucleating ligand 2,6-bis{[*N*,*N*′-bis(2-picolyl)amino]methyl}-4-*tert*-butylphenolato (bpbp$^-$) (Scheme 1) promotes an $O_2$-dependent oxidative cleavage of ketones.[2] The product carboxylates from this reaction are trapped as bridging ligands in isolated $Mn^{II}$–$Mn^{III}$ complexes. For reactions in acetone this results in a mixture of three formate/actetate-bridged $Mn^{II}$–$Mn^{III}$ complexes $[Mn_2(bpbp)(RCO_2)(R'CO_2)](ClO_4)_2$ (R = R′ = H, R = H R′ = $CH_3$ and R = R′ = $CH_3$). $^{13}$C-Labelling experiments show that the one- and two-carbon fragments of the formate and acetate bridges, respectively, are derived from acetone. The putative reactive oxidizing species derived from the combination of the $[Mn_2(bpbp)]^{n+}$ core and dioxygen has not yet been identified for this system and the present study represents a further attempt to elucidate the oxygenation reaction mechanism. Here we report several species based on the $[Mn_2(bpbp)]^{n+}$ core containing water-,

[a] Department of Physics and Chemistry, University of Southern Denmark,
Odense Campus, 5230 Odense M, Denmark
Fax: +45-6615-8780
E-mail: chk@chem.sdu.dk
[b] Westernport Secondary College,
Hastings, Victoria 3915, Australia
[c] School of Chemistry, Building 23, Monash University,
Clayton, Victoria 3800, Australia
[d] Chemistry Department, Loughborough University,
Loughborough, UK
[e] Department of Chemistry, Haverford College,
370 Lancaster Ave., Haverford, PA 19041-1392, USA
Supporting information for this article is available on the WWW under http://www.eurjic.org or from the author.

  

methanol- and THF-derived ligands in the presence and absence of $O_2$.

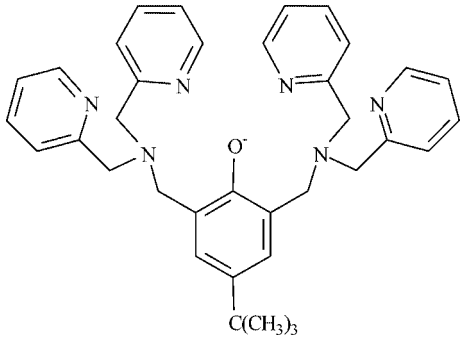

Scheme 1. 2,6-Bis{[*N*,*N*′-bis(2-picolyl)amino]methyl}-4-*tert*-butylphenolato ($bpbp^-$).

## Results and Discussion

### Air-Sensitive $Mn^{II}_2$ Complexes

The reaction of manganese(II) perchlorate with bpbpH in THF under an inert atmosphere gives a white compound formulated as $[Mn_2(bpbp)(ClO_4)_2(THF)](ClO_4)\cdot THF\cdot 3H_2O$ (**1**·$ClO_4$·THF·$3H_2O$). The cation was structurally characterised as its tetraphenylborate salt, $[Mn_2(bpbp)(ClO_4)_2(THF)][B(C_6H_5)_4]\cdot 4THF$ [**1**·$B(C_6H_5)_4$·4THF], which was obtained by recrystallisation of **1**·$ClO_4$·THF·$3H_2O$ in THF under $N_2$ in the presence of sodium tetraphenylborate. Recrystallisation of **1**·$ClO_4$·THF·$3H_2O$ in the noncoordinating solvent dichloromethane under $N_2$ resulted in replacement of the THF and terminal perchlorate ligands with adventitious water to give the complex $[Mn_2(bpbp)(ClO_4)(H_2O)_2](ClO_4)_2\cdot H_2O$ [**2**·$(ClO_4)_2$·$H_2O$].[2] The core structures of the $Mn^{II}_2$ complexes **1** and **2** are depicted in in Scheme 2 and the X-ray structures of cations **1** and **2** in Figure 1. Important bond lengths and angles are listed in Table 1. The metal coordination environments for each of the manganese ions in **1** and **2** are geometrically different. In the case of **1** this is further accentuated by the fact that the donor set on each metal ion is different. One of the tridentate 2,6-bis{[*N*,*N*′-bis(2-picolyl)amino]methyl} arms is coordinated in a facial mode while the other shows a meridional coordination geometry in both structures. The asymmetrical coordination of the bridging perchlorate is most pronounced in **2** [Mn1–O1 = 2.651(3) and Mn2–O2 = 2.334(2) Å] with a bond-length difference significantly larger than for **1** [Mn1–O7 = 2.185(18) and Mn2–O8 = 2.296(16) Å]. According to the Cambridge Crystallographic database,[3] these structures are the first reports of dimanganese complexes with a $\mu_2$-perchlorato-*O*,*O*′ bridge. Only one other example exists where a perchlorate bridges two

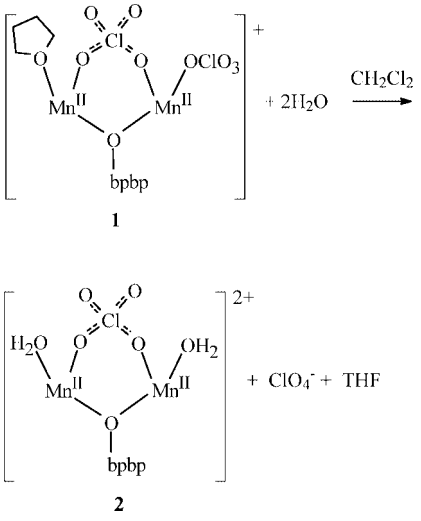

Scheme 2. Ligand-substitution reaction and core structure of the $Mn^{II}_2$ complexes **1** and **2**. For simplicity only the hinging donor O atom of the dinucleating ligand is shown. Not depicted are the three remaining N donors to each Mn ion from the heptadentate ligand.

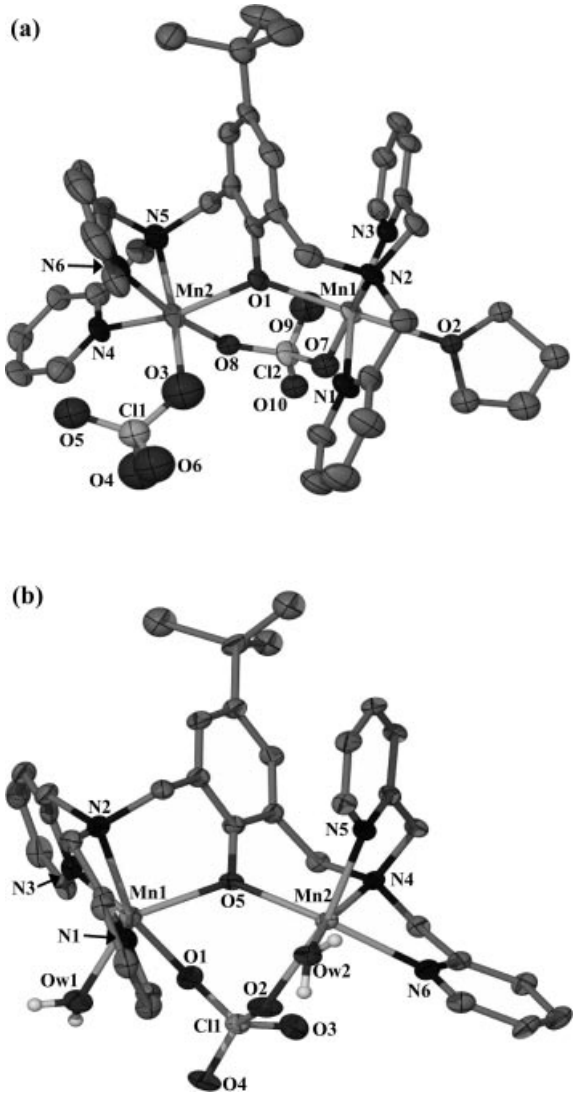

Figure 1. The X-ray crystal structures of the cations in **1** (a) and **2** (b). H atoms, except on the coordinated water molecules, have been omitted. The perchlorate counteranions and the THF molecules in **1** are modelled as disordered over two positions; only one orientation is shown.

  

Table 1. Selected bond lengths [Å] and angles [°] for **1** and **2**.

| | **1** | | **2** |
|---|---|---|---|
| Mn1–O1 | 2.135(5) | Mn1–O5 | 2.104(2) |
| Mn1–O2[a] | 2.284(16) | Mn1–Ow1 | 2.156(3) |
| Mn1–O7[a] | 2.185(18) | Mn1–O1 | 2.651(3) |
| Mn1–N1 | 2.212(7) | Mn1–N1 | 2.183(3) |
| Mn1–N2 | 2.259(6) | Mn1–N2 | 2.351(3) |
| Mn1–N3 | 2.204(6) | Mn1–N3 | 2.186(3) |
| Mn2–O1 | 2.130(5) | Mn2–O5 | 2.113(2) |
| Mn2–O3 | 2.213(16), 2.056(15) | Mn2–Ow2 | 2.123(3) |
| Mn2–O8[a] | 2.296(16) | Mn2–O2 | 2.334(2) |
| Mn2–N4 | 2.271(6) | Mn2–N6 | 2.239(3) |
| Mn2–N5 | 2.287(7) | Mn2–N4 | 2.295(3) |
| Mn2–N6 | 2.224(8) | Mn2–N5 | 2.248(3) |
| Mn1···Mn2 | 3.8620(17) | Mn1···Mn2 | 3.8044(7) |
| Mn1–O1–Mn2 | 129.8(3) | Mn1–O5–Mn2 | 128.91(10) |

[a] Bond lengths for the disordered bridging perchlorate and THF molecule in **1** are given as an average whenever the Mn–O bond lengths were not significantly different (bond difference less than $3\cdot\sqrt{[(\sigma_1)^2 + (\sigma_2)^2]}$).

manganese atoms, but in this case the perchlorate acts as a one-atom bridge ($\mu_2$-perchlorato-*O*,*O*).[4]

## Air Oxidation of the $Mn^{II}_2$ Complexes

Solutions of complexes **1** and **2** in water, methanol, acetone and THF darken within minutes on exposure to air. In acetone, this occurs with concomitant acetone oxidation.[2] The species we have now identified when air oxidation of **1** is carried out in water, methanol or THF are summarised in Scheme 3. The dinuclear, mixed-valence $Mn^{II}$–$Mn^{III}$ complex $[Mn_2(bpbp)(CH_3O)_2(H_2O)_2](ClO_4)_2$ [**3**·$(ClO_4)_2$] and the tetranuclear complex $[Mn_4(O)_{4-n}(OH)_n(bpbp)_2](ClO_4)_4$ ($n$ = 1 or 2) [**7**·$(ClO_4)_4$], were isolated from methanol and THF, respectively, as their perchlorate salts. Exposure of the salts of **1** and **2** as solid compounds to air results in them turning brown within hours. We have not determined the nature of this solid-state reaction.

## The Solid-State Characterisation

### *X-ray Structures*

The dark-green crystals obtained from the air oxidation of **1** in methanol are the mixed-valence $Mn^{II}$–$Mn^{III}$ complex **3**·$(ClO_4)_2$ (Figure 2). This complex is identical to the product of the methanol reaction of manganese perchlorate with bpbpH in air without isolating an intermediate $Mn^{II}$–$Mn^{II}$ complex.[5] The two exogenous H-bonded methoxo-aquo "bridging groups" span the metal ions. The complex is unsymmetrical and the valence trapping unambiguous: the two methoxide ligands are coordinated to the $Mn^{III}$ ion with an average $Mn^{III}$–O distance of 1.876 Å, while the two $Mn^{II}$–$OH_2$ distances are an average of 0.279 Å longer.

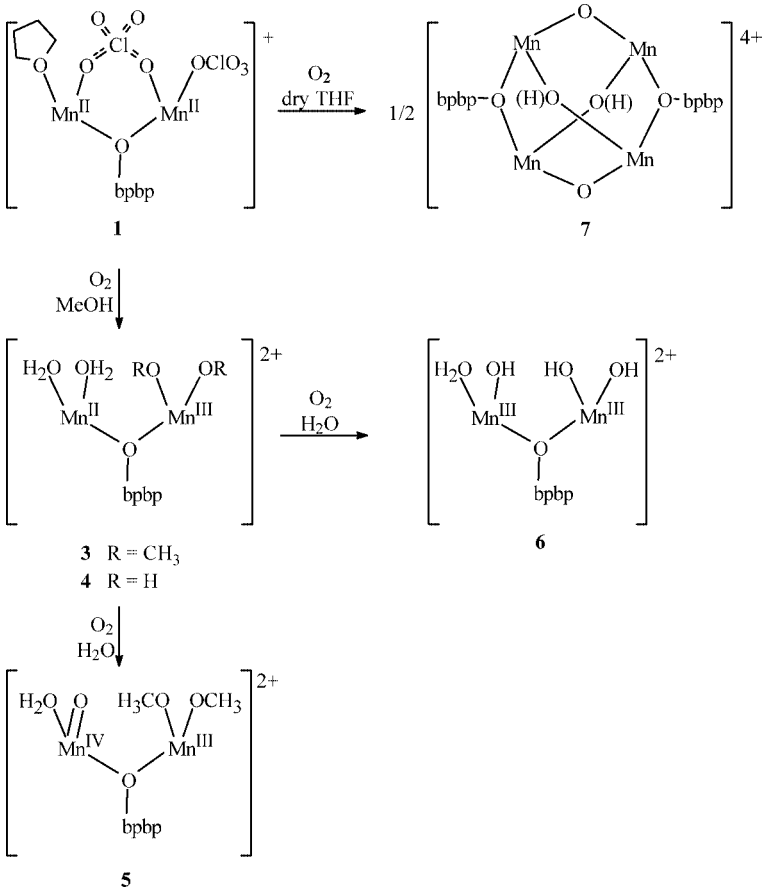


Scheme 3. The core structures of the starting compound **1** and the complexes isolated or identified by ESI MS.

  

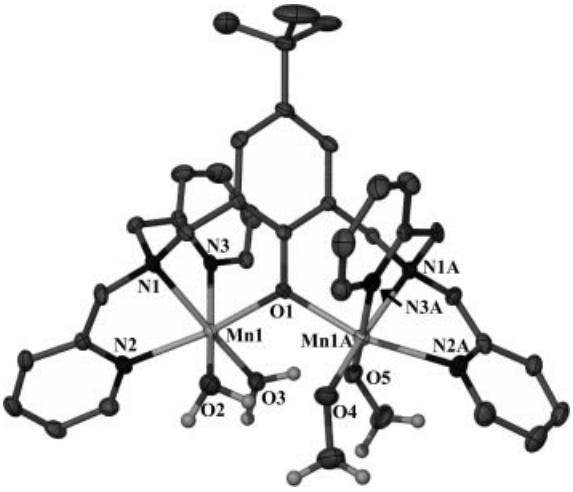


Figure 2. The X-ray crystal structure of the cation in **3**.

Solutions of **1** in THF turn dark in minutes and deposit brown-black solids in good yields over some hours. Addition of *tert*-butylhydrogen peroxide to the reaction results in an instant colour change and precipitation of a dark solid. The products isolated by these two synthetic routes give identical elemental analyses consistent with two $ClO_4^-$ ions per $[Mn_2(bpbp)]^{n+}$ unit. These products look to be amorphous and give no detectable powder XRD pattern. However, on one occasion crystals were obtained by the complete evaporation of the THF from a very dilute solution in a flask with a large surface area at the base. We have not been successful in growing better crystals under a variety of more appropriate conditions. The structure of these small ($0.20 \times 0.10 \times 0.02$ mm), weakly diffracting brown crystals was determined by synchrotron X-ray crystallography to be a tetranuclear, adamantane-type manganese complex [**7**·$(ClO_4)_4$; Figure 3]. The data are of low quality, although the core topology is clear. Bond lengths and angles are listed in Table 2. A definitive oxidation-state assignment cannot be made from the X-ray structure alone since the poor data quality precludes conclusive determination of the protonation state of the cation. The charge of the cation (4+) is without doubt, however, and the overall oxidation state can therefore in theory range from $Mn^{III}_2Mn^{IV}_2$ (only oxide bridges) down to $Mn^{II}_2Mn^{III}_2$ (only hydroxide bridges); lower oxidation-state assignments would require $H_2O$ as bridging ligand or protonation of the bridging phenolate, both of which are unfeasible.

We eliminated the lower oxidation-state formulations $[Mn^{II}Mn^{III}_3(O)(OH)_3(bpbp)_2]^{4+}$ and $[Mn^{II}_2Mn^{III}_2(OH)_4(bpbp)_2]^{4+}$ on the basis of a comparison of metric parameters with known compounds (see below). This leaves three possible assignments depending on the number of hydroxide bridges, namely $[Mn^{III}_4(O)_2(OH)_2(bpbp)_2]^{4+}$, $[Mn^{III}_3Mn^{IV}(O)_3(OH)(bpbp)_2]^{4+}$ and $[Mn^{III}_2Mn^{IV}_2(O)_4(bpbp)_2]^{4+}$. Notably, the structure of complex **7** is very similar to its $Fe^{III}_4$ counterpart $[(bpbp)_2Fe^{III}_4(\mu\text{-}O)_2(\mu\text{-}OH)_2](ClO_4)_4$,[6] thus implying that an isostructural **7** might also contain two hydroxide bridges and hence the same metal oxidation state, i.e. $Mn^{III}_4$. Both complexes have identical metal–$O_{phenoxo}$ distances [Fe–$O_{phenoxo}$ = 2.092(4), Mn–$O_{phenoxo}$ = 2.095(7) Å], although the average Fe–$O_{oxo/hydroxo}$ distance [1.893(5) Å] is slightly longer than

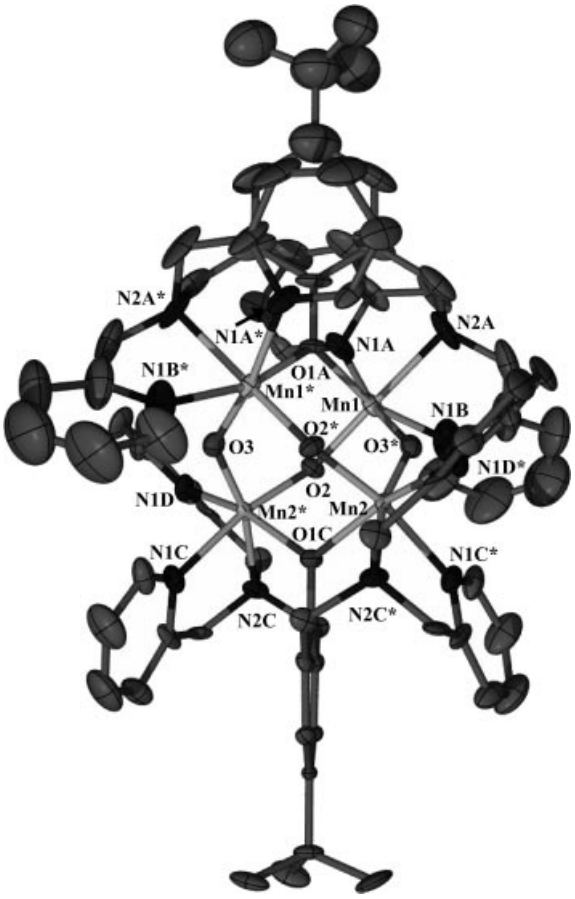


Figure 3. The X-ray crystal structure of the cation in **7**.

Table 2. Selected bond lengths [Å] and angles [°] for **7**. Symmetry transformations used to generate equivalent atoms as indicated by *: $-x$, $y$, $1/2 - z$.

| | | | |
|---|---|---|---|
| Mn1–Mn2* | 3.404(3) | Mn1–Mn1* | 3.664(5) |
| Mn1–Mn2 | 3.429(3) | Mn2–Mn2* | 3.648(4) |
| Mn1–O2 | 1.848(10) | Mn2–O3 | 1.818(11) |
| Mn1–O3* | 1.852(11) | Mn2–O2 | 1.864(11) |
| Mn1–O1A | 2.089(6) | Mn2–O1C | 2.100(7) |
| Mn1–N1A | 2.105(14) | Mn2–N1C | 2.119(14) |
| Mn1–N2A | 2.153(14) | Mn2–N2C | 2.149(14) |
| Mn1–N1B | 2.174(16) | Mn2–N1D | 2.215(12) |
| Mn1*–O1A–Mn1 | 122.6(6) | Mn1–O2–Mn2 | 135.0(6) |
| Mn2*–O1C–Mn2 | 120.6(6) | Mn2–O3–Mn1* | 136.1(6) |
| O2–Mn1–O3* | 98.1(5) | O3–Mn2–O2 | 99.3(5) |
| O2–Mn1–O1A | 99.1(4) | O3–Mn2–O1C | 100.0(4) |
| O3*–Mn1–O1A | 90.8(4) | O2–Mn2–O1C | 90.7(4) |
| O2–Mn1–N1A | 92.4(5) | O3–Mn2–N1C | 91.5(6) |
| O1A–Mn1–N1A | 85.5(5) | O1C–Mn2–N1C | 84.0(4) |
| O3*–Mn1–N2A | 90.7(6) | O2–Mn2–N2C | 90.9(5) |
| O1A–Mn1–N2A | 88.9(6) | O1C–Mn2–N2C | 89.0(4) |
| N1A–Mn1–N2A | 79.3(6) | N1C–Mn2–N2C | 79.1(6) |
| O2–Mn1–N1B | 96.7(6) | O3–Mn2–N1D | 96.0(5) |
| O3*–Mn1–N1B | 90.4(6) | O2–Mn2–N1D | 89.7(5) |
| N1A–Mn1–N1B | 90.4(7) | N1C–Mn2–N1D | 92.6(5) |
| N2A–Mn1–N1B | 74.9(7) | N2C–Mn2–N1D | 74.8(5) |

  

the equivalent distance in **7** [Mn–$O_{oxo/hydroxo}$ = 1.846(11) Å].

Jahn–Teller distortions are commonly observed in pseudo-octahedral high-spin $Mn^{III}$ ($d^4$) complexes; these distortions usually take the form of axial elongations or compressions. In the case of the manganese in complex **7**, the principal distortion is caused by the shorter bond lengths on one octahedral face due to the anionic oxygen-based ligands. In addition, there is an axial elongation in that the longest Mn–O bond is *trans* to the longest Mn–N bond. These effects are, however, too subtle to be used for oxidation,state assignment.

The majority of $Mn_4$ adamantane-type complexes with which **7** can be compared have been prepared using neutral tridentate capping ligands [e.g. 1,4,7-triazacyclononane, tris-(aminomethyl)ethane or *N*,*N*-bis(2-pyridylmethyl)ethylamine] and the oxygen atom bridging groups are all non-protonated oxides rather than hydroxides.[7,8] The strength of the $Mn^{IV}$–oxo bond typically yields robust adamantane $Mn^{IV}_4O_6$ cores with more or less unambiguous spectroscopic signatures. Two singly protonated[7d] complexes and two one-electron-reduced[7e,8] complexes derived from the $Mn^{IV}_4O_6$ core have been structurally characterised. Ligand-exchange reactions have furthermore yielded neutral bis-ligand complexes containing two *N*,*N*-bis(2-pyridylmethyl)-ethylamine ligands and two *N*-substituted iminodiacetate ligands.[7f] Typical geometrical parameters for these complexes are $Mn^{IV}$–O ≈ 1.80, $Mn^{IV}$–OH ≈ 1.95, $Mn^{III}$–O ≈ 1.83 Å and Mn–O–Mn ≈ 128–130°. Only small differences in the Mn–O bond length arise from reduction of $Mn^{IV}$ to $Mn^{III}$, while protonation induces significant changes. Only one other $Mn_4$ complex with an adamantane core incorporating bridging alkoxides/phenoxides as in **7** is known.[8] Armstrong and co-workers have shown that the mixed-valence complex $[(tphpn)_2Mn^{III}Mn^{IV}{}_3(\mu\text{-}O)_4](OTf)_2(ClO_4)_3$ [Htphpn = *N*,*N*,*N*′,*N*′-tetrakis(2-pyridylmethyl)-2-hydroxypropane-1,3-diamine] is formed by a core rearrangement induced by a one-electron oxidation of the $[\{(tphpn)Mn^{III}Mn^{IV}(\mu\text{-}O_2)\}_2]^{4+}$ dimer-of-dimers complex.[8] The complex contains four oxide and two alkoxide bridges and the average Mn–$O_{oxo}$ bond length is 1.805(8) Å, which corresponds well to a 3:1 mixture of $Mn^{IV}$ and $Mn^{III}$ with all oxide bridges. The analogous average Mn–$O_{oxo/hydroxo}$ bond length for **7** is 1.846(11) Å, which is slightly longer and therefore consistent with a lower average oxidation state in **7**.

### *Oxidation-State Assignment by Bond Valence Sum (BVS) Analysis*

To further assess the possible oxidation states of Mn in **7**, we employed Bond Valence Sum (BVS) analysis,[9] which uses all of the metal–ligand bond lengths to indicate the likely oxidation state. Each bond length is used to calculate a bond valence from the expression BV = exp[($r_0$ – $r_{MX}$)/0.37 Å], where $r_0$ depends on the identity of M and X. The traditional but cumbersome approach[9] to oxidation-state determination by BVS assumes that the $r_0$ values also depend on the oxidation state of M, and these $r_0$ values are selected so that, for complexes with unambiguous oxidation states, the BVS is approximately equal to the oxidation state. This approach requires a separate calculation for each possible oxidation state and is unsuited for mixed-valence complexes. An alternative, and simpler, approach[10] uses the BVS calculated with oxidation-state-independent $r_0$ but allows that it may deviate for some specific donors. For example, the parameters $r_0$(M–O) = 1.759, $r_0$(M–N) = 1.831 and $r_0$(M–S) = 2.151 Å can distinguish between complexes of high-spin iron(II) (BVS = 2.30 ± 0.14), high-spin iron(III) (BVS = 3.04 ± 0.12), and low-spin iron [BVS = 4.2 ± 0.3 for low-spin iron(II or III)].

Calculations of BVSs using data from mononuclear manganese complexes found in a search of the Cambridge Structural Database[3] indicate that the same $r_0$ parameters previously used for iron can be used to distinguish high-spin manganese oxidation states (Figure 4). The BVSs for mononuclear manganese complexes with oxidation states specified in the CSD name show a clear separation between manganese(II), (III) and (IV) complexes. About 5% of the "manganese(II)" complexes have BVSs greater than 2.5 (i.e. closer to values expected for $Mn^{III}$ or $Mn^{IV}$), but upon consulting the original literature these were found either to be misnamed in the CSD (NOTGUY, HOSTUE, WAQDEX, RULNER), oxidation-state ambiguous (SEVWOF), or likely intermediate-spin (HODTUP, MNPHCY02, TOGPEK) or low-spin (NTPOMN, NTPIPM10, LAHCUS, GOGBEJ, YEXWAZ, WEGQII, LIHBEJ) complexes. Excluding these from the manganese(II) data results in 279 complexes with BVS = 1.92 ± 0.17. Thus, we conclude that high-spin $Mn^{II}$, $Mn^{III}$ and $Mn^{IV}$ complexes have a BVS of approximately 1.9, 3.1 and 4.1 ± 0.2, respectively, when using the $r_0$ values previously used for iron complexes.

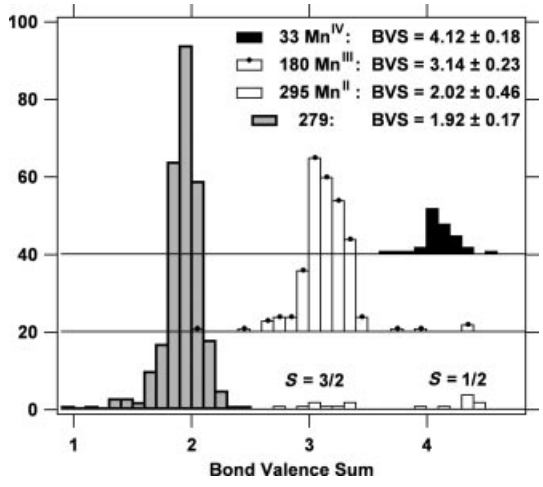


Figure 4. BVSs calculated from bond lengths in the Cambridge Structure Database (April 2001 release) for mononuclear manganese complexes (crystallographic $R < 0.10$) with only N, O and S coordination in which the oxidation state of the manganese (II, III or IV) is specified in the name field. BVS analyses in this paper use $r_0$ values of 1.759, 1.831 and 2.151 Å for Mn–O, Mn–N and Mn–S bonds, respectively.

  

Figure 5 shows that most binuclear manganese complexes in the CSD have BVSs that are within 0.2 of the average BVS expected from the assigned oxidation states. Most of the outliers shown in Figure 5 (those with CSD codes shown) can be explained as due to errors in oxidation state naming or differences in spin state, as explained in the figure caption.

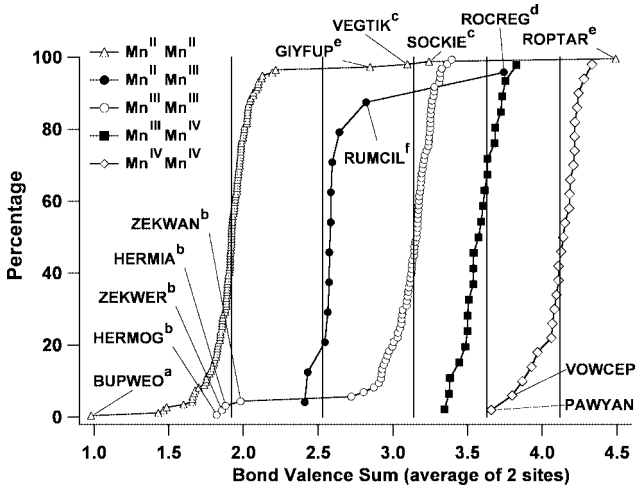


Figure 5. BVSs calculated for dinuclear manganese complexes where the oxidation states are specified by the name in the Cambridge Structure Database (April 2001 release) plotted vs. the percentile within each class. The five solid lines indicate, from left, the BVSs expected for (II,II), (II,III), (III,III), (III,IV) and (IV,IV) dinuclear complexes. CSD codes are indicated for structures with especially large deviations from the expected BVS. In most cases, the large deviations were explained upon inspection of the CSD record: (a) only 42% occupancy of manganese atoms; (b–d) misassigned oxidation states in name should be (b) $Mn^{II}Mn^{II}$, (c) $Mn^{III}Mn^{III}$ and (d) $Mn^{III}Mn^{IV}$; (e) probable low- or intermediate-spin $Mn^{III}$; ambiguous oxidation state due to presence of cobalt atom in cluster (assigned as $Co^{2+}$).

Using the same oxidation-state-independent $r_0$ values, the BVSs of the $Mn^{II}_2$ complexes **1**·$ClO_4$·THF·$3H_2O$ and **2**·$ClO_4$·$H_2O$ as well as the $Mn^{II}$–$Mn^{III}$ complex **3**·$(ClO_4)_2$ were calculated; they are listed in Table 3. There is excellent agreement with the values expected based on the data of Figures 4 and 5. From the BVSs of the individual Mn atoms of **3** it is clear that they are valence-trapped as a $Mn^{II}$ and $Mn^{III}$. The BVS of complex **7**·$(ClO_4)_4$, when compared to the values obtained by analysis of three X-ray structures of closely related $Mn^{III}Mn^{IV}_3$ and $Mn^{IV}_4$ adamantane core complexes, shows that **7** clearly has a much lower overall oxidation state. The average BVS (3.25) is equally consistent with a $Mn^{III}_4$ (expected $3.14 \pm 0.2$) or $Mn^{III}_3Mn^{IV}$ (expected $3.38 \pm 0.2$) core. The possibility of a $Mn^{III}_2Mn^{IV}_2$ dimer (expected BVS = $3.63 \pm 0.2$) is, however, much less likely.

### *Oxidation-State Assignment by XANES*

XANES of **1**·$ClO_4$·THF·$3H_2O$ and **7**·$(ClO_4)_4$ supports these oxidation-state assignments (see Figure 6). The edge energy, which we consider to be the energy at which the XANES spectrum intensity = 0.5, for **1**·$ClO_4$·THF·$3H_2O$ is almost identical to the energy recorded for $Mn^{II}(acac)_2$, thus confirming the oxidation-state assignment. The edge energy for **7**·$(ClO_4)_4$ is very close to that measured for $Mn^{III}(acac)_3$, thus indicating that the overall oxidation state of **7**·$(ClO_4)_4$ might be $Mn^{III}_4$. Furthermore, the edge energy is markedly lower than that found in the mixed-valent manganese(III,IV) complex $[tpa_2Mn_2O_2](ClO_4)_3$ [tpa = tris(2-pyridylmethyl)amine; lower by 1.5 eV] and the manganese(IV) complex $[(Me_3tacn)_2Mn_2O_3][PF_6]_2$ ($Me_3tacn$ = 1,4,7-trimethyl-1,4,7-triazacyclononane; lower by 3.0 eV). The large difference between the edge energy of **7**·$(ClO_4)_4$ and the mixed-valence tpa-manganese(III,IV) complex discounts a $Mn^{III}_2Mn^{IV}_2$ oxidation-state assignment for **7**·$(ClO_4)_4$. The difference in edge energy between a $Mn^{III}_3Mn^{IV}$ and a $Mn^{III}_4$ complex is, however, probably too small to be discerned by XANES, and these two oxidation-state assignments can therefore not be excluded for **7**·$(ClO_4)_4$.

Assignment of an oxidation state of $Mn^{III}_2Mn^{IV}_2$, and thus oxo bridges, for **7** has inherent problems due to its lack of solution stability, as indicated by the lack of Mn–O CT absorptions and $Mn_4$ ions in the ESI mass spectrum (see below). This contrasts with the data for the counterpart $Fe^{III}_4$ complex,[6] for which, for example, an ion assignable to the singly deprotonated species $[(bpbp)_2Fe^{III}_4(O)_3(\mu\text{-}OH)]^{3+}$ is easily observed. This is contradictory to the typical stability of oxo-bridged manganese complexes. The presence of hydroxo bridges, which typically are weaker than oxo bridges, can account for the instability of **7**·$(ClO_4)_4$ along with the fact that $Mn^{III}$–O bonds are believed to be more labile than $Mn^{IV}$–O bonds due to Jahn–Teller effects.[7e] Armstrong and co-workers have further shown that

Table 3. Values obtained for the oxidation state assignment from a BVS analysis of **1**, **2**, **3** and **7**.

| | BVS analysis for crystallographically unique Mn atoms | | | | Av. BVS | Oxidation state assignment | Theoretical av. BVS[a] |
|---|---|---|---|---|---|---|---|
| **1**·$ClO_4$·THF·$3H_2O$ | 1.84 | | 1.91 | | 1.87 | $Mn^{II}_2$ | $1.9 \pm 0.2$ |
| **2**·$ClO_4$·$H_2O$ | 1.96 | | 1.90 | | 1.93 | $Mn^{II}_2$ | $1.9 \pm 0.2$ |
| **3**·$(ClO_4)_2$[5] | 3.07 | | 2.02 | | 2.54 | $Mn^{II}Mn^{III}$ | $2.5 \pm 0.2$ |
| **7**·$(ClO_4)_4$ | 3.27 | | 3.24 | | 3.25 | $Mn^{III}_4$ | $3.1 \pm 0.2$ |
| | | | | | | ($Mn^{III}_3Mn^{IV}$) | ($3.4 \pm 0.2$) |
| $[Mn_4(\mu\text{-}O)_6(bpea)_4]^{4+}$ [7e] | 3.99 | 4.03 | 3.97 | 4.14 | 4.03 | $Mn^{IV}_4$ | $4.1 \pm 0.2$ |
| $[Mn_4(\mu\text{-}O)_6(bpea)_4]^{3+}$ [7e] | 4.01 | 4.05 | 3.66 | 3.89 | 3.90 | $Mn^{III}Mn^{IV}_3$ | $3.9 \pm 0.2$ |
| $[Mn_4(\mu\text{-}O)_4(tphpn)_4]^{5+}$ [8] | 4.06 | 3.80 | 4.13 | 3.69 | 3.92 | $Mn^{III}Mn^{IV}_3$ | $3.9 \pm 0.2$ |

[a] BVS values used: 1.9, 3.1 and $4.1 \pm 0.2$ for $Mn^{II}$, $Mn^{III}$ and $Mn^{IV}$ respectively. bpea = *N*′*N*-bis(2-pyridylmethyl)ethylamine; Htphpn = *N*,*N*,*N*′,*N*′-tetrakis(2-methylpyridyl)-2-hydroxypropanediamine. Bond lengths used for BVS analysis of **1**, **2** and **7** can be found in Tables 1 and 2; for structural data for the remaining complexes see the references given in brackets.

  

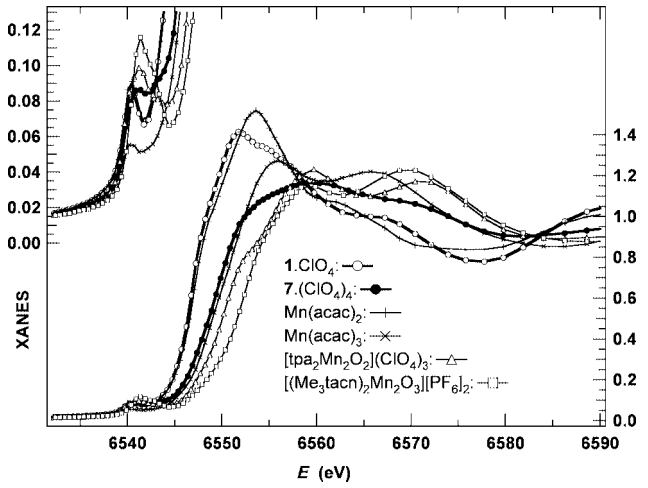


Figure 6. Comparison of Mn K-edge XANES spectra for **1**·$ClO_4$ and **7**·$(ClO_4)_4$ with those of $Mn^{II}$ and $Mn^{III}$ complexes of acetylacetonate (acac), a $Mn^{III}Mn^{IV}$ mixed-valence di-oxo-bridged complex of tris(2-pyridylmethyl)amine (tpa), and a $Mn^{IV}$ dimeric tri-oxo-bridged complex of 1,4,7-trimethyl-1,4,7-triazacyclononane ($Me_3tacn$).

the effective basicity of the oxo bridges in $[Mn_4O_6(bpea)_4]^{4+}$ increases by 17.5 orders of magnitude upon one-electron reduction.[7e] Thus, the presence of one or two hydroxo bridges in **7** is very feasible.

On the basis of the crystal structure (BVS analysis), elemental analysis and XANES of **7**·$(ClO_4)_4$, we therefore propose that the complex might be $[Mn_4(O)_{4-n}(OH)_n(bpbp)_2]^{4+}$ ($n$ = 1 or 2) and contain either three or four $Mn^{III}$ centres.

## The Structural Formulation of the Solution- and Gas-Phase Species Derived from Hydroxylic Solvents by Analysis of ESI Mass Spectra

Tractable products were not isolated after the air oxidation of **1** in water or in methanol containing significant amounts of water. Analyses of fragmentation pathways in ESI mass spectrometric studies of reaction solutions indicate that aqueous solutions contain the homologue of **3**, the $Mn^{II}$–$Mn^{III}$ $[Mn_2(bpbp)(OH)_2(H_2O)_2]^{2+}$ ion (**4**), and higher oxidation state $Mn^{III}_2$ and $Mn^{III/IV}_2$ solvent-derived species. The presence of methoxide vs. hydroxide most likely facilitates the isolation of **3**. Terminal methoxide ligands are more commonly characterised for $Mn^{III}$ and $Fe^{III}$ complexes than hydroxide ligands, presumably because proton-transfer interactions between the hydroxide ligand and solvent (non-coordinated) water are blocked. Mn compounds with terminal hydroxide ligands are usually characterised only when the hydroxide is found in cavities and other well-shielded environments.[11] A comparison of the ESI mass spectra of **3**·$(ClO_4)_2$ using both methanol and water as spray solvent is shown in Figure 7. Figure 7(a) and (e) show that similar spectra are obtained for **3**·$(ClO_4)_2$ in methanol and water, respectively, under standard source conditions. Through a series of Collision Activation Dissociation (CAD) experiments we were able to show that the ion at $m/z$ 348.8, which is observed as essentially the only species in both these mass spectra, can be assigned to the $Mn^{II}$–$Mn^{III}$ oxide $[Mn_2(bpbp)(O)]^{2+}$ (**8**). Cation **8** is, however, most likely *not* found solution. This ion corresponds to the loss of the mass equivalent of two water molecules and one dimethyl ether molecule from **3**, or the loss of the mass equivalent of three water molecules from **4**, to give **8**. The gas-phase fragmentation pathway to **8** could be mapped from spectra recorded using very mild source conditions [Figure 7(b) and (f)]. We assigned the higher oxidation state species $[Mn^{III}_2(bpbp)O(OH)_2]^{2+}$ ($m/z$ 357.2) and $[Mn^{III/IV}_2(bpbp)O(OH_2)(OCH_3)_2]^{2+}$ (**5**) ($m/z$ 388.7) to the ions generated from the water solutions under mild source conditions. Coordinated water ligands are retained by cations **3** and **4** in the spectra in Figure 7(b) and (f), which show also that methoxide ligands can be substituted by hydroxides. Assignments for the various ions are listed under the spectra. Only neutral species can be lost from cations in gas-phase CAD experiments: coordinated water loss is facile, and the mass equivalents of hydroxyl and methoxyl radicals and dimethyl ether can also be lost, ultimately to produce cation **8**. The pathways are delineated in the scheme under the spectra in Figure 7. We have previously noted the facile gas-phase formation of (sometimes novel) metal oxide ions from metal carbonates by loss of neutral $CO_2$.[12] The present cases showing mass losses equivalent to the neutral fragments $H_2O$, $CH_3OCH_3$, $HO^{\cdot}$ and $CH_3O^{\cdot}$ serve as another example.

## Magnetic Susceptibility

The magnetic susceptibility of **3**·$(ClO_4)_2$ was measured in the temperature range 4.2 to 300 K at an applied field of 1 T. The data are generally indicative of weak antiferromagnetic coupling occurring within $Mn^{II}/Mn^{III}$ pairs via the endogenous bridging phenolate group of $bpbp^-$. The strong H-bonding between the two aqua ligands of the $Mn^{II}$ and the two methoxide ligands of the $Mn^{III}$ may also contribute a superexchange pathway. Least-squares fitting of the susceptibility data to Heisenberg exchange models ($-2J\ S_1 \cdot S_2$) for $S$ = 5/2:4/2 pairs, assuming the $g$ values for $Mn^{II}$ and $Mn^{III}$, are the same and give the best fit parameters $g = 1.97 \pm 0.02$ and $J = -3.7 \pm 0.02\ cm^{-1}$. The experimental and calculated plots are shown in Figure 8. The $J$ value is similar to those found for other dinuclear $Mn^{II}$–$Mn^{III}$ μ-phenoxo complexes but does not agree with the structural correlation found by Latour et al.[13] for μ-phenoxo, bis-μ-carboxylato compounds, largely because the $Mn^{II}$–O and $Mn^{III}$–O(phenoxo) lengths are so similar in the present compound.

Magnetic susceptibility and variable-field magnetisation measurements on samples of the bulk materials of **7**·$(ClO_4)_4$ were also carried out. The plot of effective magnetic moment ($\mu_{eff}$) vs. temperature, measured in a field of 1 T, is shown in Figure 9, while the isothermal magnetisation data are given in Figure S1 (Supporting Information). A stronger magnetic coupling is evident from the overall

  

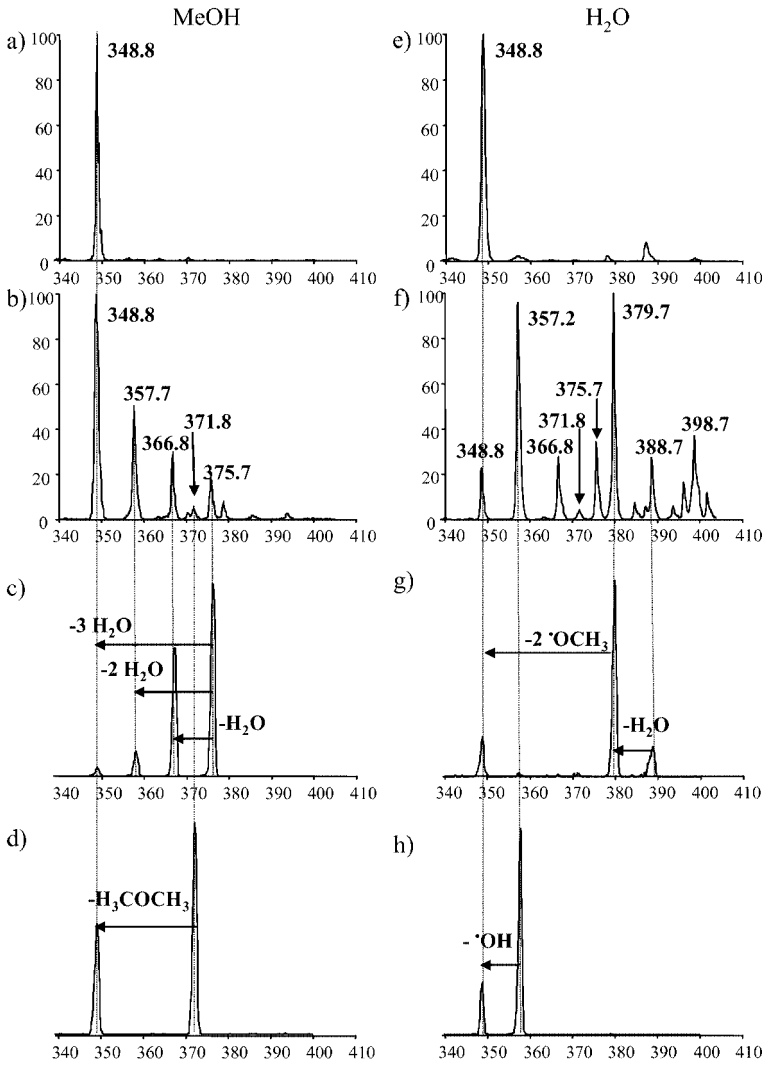


Figure 7. ESI mass spectra of **3**·$(ClO_4)_2$ in methanol (a and b) and in water (e and f). Spectra (a) and (e) were recorded with a tube lens potential of 100 V (normal source conditions); spectra (b) and (f) were recorded with a tube lens potential of 20 V (mild source conditions). Collision-Activated Dissociation (CAD) spectra (c, d and g, h) were recorded by mass selection from spectra (b) and (f), respectively. Mass selected for CAD: (c) *m*/*z* 375.7; (d) *m*/*z* 371.8; (g) *m*/*z* 388.7; (h) *m*/*z* 357.2. Peak assignment and CAD pathways are show below spectra.

  

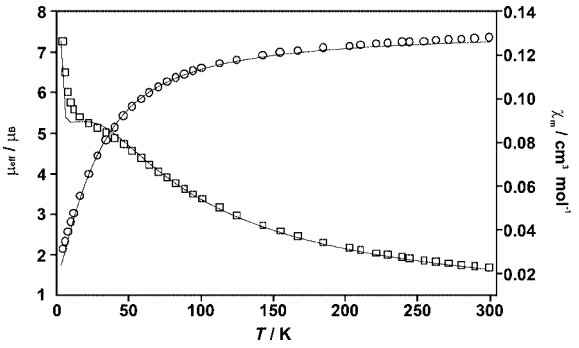


Figure 8. Plots of magnetic susceptibility () and moment (O) per molecule for complex **3**·$(ClO_4)_2$. The solid lines are the calculated values with the $S$ = 5/2:4/2 model and parameters given in the text.

lower magnetic moment per manganese ion in bulk samples of **7**·$(ClO_4)_4$ compared with **3**·$(ClO_4)_2$. This suggests a superexchange pathway that is more efficient than that in **3** and is consistent with the presence of oxo bridges, although in the absence of more a definitive oxidation state assignment from the X-ray crystal structure and XANES measurements a precise analysis cannot be made. We interpret the data as follows. At 300 K, a $\mu_{eff}$ value of 8.2 $\mu_B$ per $Mn_4$ is obtained, and this decreases gradually to reach 7.7 $\mu_B$ at 30 K, followed by a rapid decrease to reach 5.6 $\mu_B$ at 2 K, from where it continues to decrease. Four uncoupled $Mn^{III}$ $S$ = 2 centres would give a $\mu_{eff}$ of 9.8 $\mu_B$ ($g$ = 2.0), thus medium strength antiferromagnetic coupling is indicated. Except for the beginning of the region of rapid decrease (10–5 K), the $\mu_{eff}$ vs. temperature data can be fitted well to a three-$J$ ($S$ = 2) tetramer ($-2JS_1 \cdot S_2$) model[14] [for atoms Mn(1), Mn(2), Mn(3) and Mn(4), where Mn(3) is Mn(2′) and Mn(4) is Mn(1′) in Figure 3], with $g$ = 1.94 and $J_{12}$ = –8, $J_{13}$ = –38 and $J_{24}$ = 23 $cm^{-1}$. The $J_{13}$ and $J_{24}$ values could be positive or negative for a similar $J_{12}$ value to that shown (see Figure 9, dotted line). This is not the same as using a two-$J$ model with $J_{13} = J_{24}$ as such a model does not give a good fit of the data. Comparison of these $J$ values to those previously reported for $Mn^{III}$–O–$Mn^{III}$- (angular) and $Mn^{III}$–(OPh)–$Mn^{III}$-bridged systems unfortunately does not give an unambiguous assignment of the individual $J$ values to particular bridges in the adamantane core. This is because the $J$ values found for such bridges often overlap in size and are not as clearly defined as in analogous $Fe^{III}$ systems. In support of the fitting using three $J$ values, it should be noted that the best fit to the data for the isostructural, and possibly isovalent, $Fe^{III}_4$ complex was a three-$J$ value fit.[6] In that case they were readily assigned to the three types of bridge. The magnetisation isotherm for **7**·$(ClO_4)_4$, at 2 K (Figure S1), did not reach saturation in $M$ at the highest field of 5 T, but gave a value of 7.65 $\mu_B$, which is somewhere between $S$ = 3 and $S$ = 4 ground-state values. The best-fit parameter set, given above, gave a calculated $M$ value, at 2 K and 5 T, of 6.9 N$\mu_B$, which is less than the observed value. This discrepancy may be related to the heterogeneity of the sample used. The energy levels calculated from this parameter set show $S$ = 3 lower, but only by 4 $cm^{-1}$, than $S$ = 4, with other $S$ values greater than 100 $cm^{-1}$ above. It was also possible to obtain reasonable fits to the data of Figure 9 using a $Mn^{II}Mn^{III}Mn^{II}Mn^{III}$ model with spins {5/2, 2, 5/2, 2}, and a similar ground $S$ = 3 state and nearby $S$ = 4, but this formulation is unlikely in view of the XANES data.

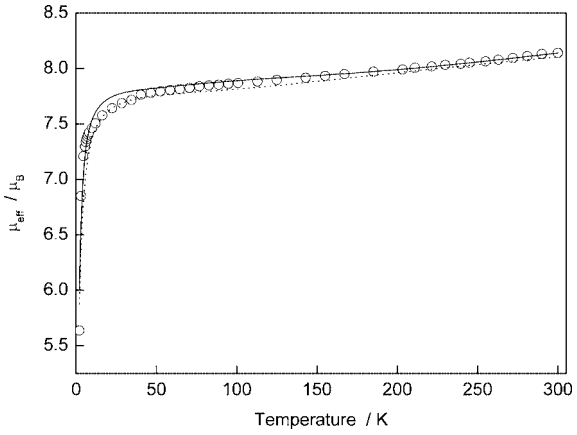


Figure 9. Plot of magnetic moment, $\mu_{eff}$, (open circles) vs. temperature, per $Mn_4$, for **7**·$(ClO_4)_4$. The solid line is that calculated using the parameters for the $Mn^{III}_4$ model, with $g$ = 1.94, $J_{12}$ = –8 $cm^{-1}$, $J_{13}$= –38 $cm^{-1}$ and $J_{24}$ = 23 $cm^{-1}$. The dotted line uses parameters, also for the $Mn^{III}_4$ model, with $g$ = 1.93, $J_{12}$ = –14 $cm^{-1}$, $J_{13}$ = 66 $cm^{-1}$ and $J_{24}$ = –67 $cm^{-1}$.

## Conclusions

Dioxygen-sensitive dimanganese(II) complexes of a pentadentate, phenoxide-hinged, dinucleating ligand with labile solvent-derived and perchlorate exogenous ligands have been structurally characterised. In previous work we have shown that the $[Mn^{II}_2(bpbp)]^{3+}$ cation can activate dioxygen in an as-yet-unknown mechanism to form an oxidant capable of oxidative ketone cleavage. Using other solvents we show here that reactions with $O_2$ yield a series of dinuclear $Mn^{II}$–$Mn^{III}$, $Mn^{III}_2$ and $Mn^{III}$–$Mn^{IV}$ complexes and one tetranuclear manganese complex. However, we cannot propose that any of these species is the pertinent $[Mn^{II}_2(bpbp)]^{3+}/O_2$-derived oxidant. The use of "anhydrous" conditions was crucial for obtaining the crystals of **1**, **2**, **3** and **7**. The structures of the solution species **4**, **5** and **6** have been predicted on the basis of the information provided by the crystal structures of the other members of the series and through a careful analysis of tandem MS experiments. The ESI MS studies indicate facile formation of a gas-phase oxide species **8**. Without the analysis of MS/MS under mild source conditions here, and knowledge of the solid-state structures of the precursors, such a species might otherwise have been mistaken as being present in solution.

The range of oxidation states attainable for an adamantane $Mn_4O_6$ core has been extended to a lower oxidation state in complex **7**. By comparison with known oxo-bridged, tetramanganese adamantane core complexes, as well as the use of BVS analysis and XANES measurements, the overall oxidation state of complex **7** has been narrowed

  

down to two possible assignments – $[Mn^{III}_4(O)_2(OH)_2(bpbp)_2]^{4+}$ and $[Mn^{III}_3Mn^{IV}(O)_3(OH)(bpbp)_2]^{4+}$. The difficulty in obtaining solution spectroscopic data, and thus further oxidation-state evidence, can be attributed to the expected reactivity of the $Mn^{III}$–OH–$Mn^{III}$ moieties and serve as further circumstantial evidence that **7** is not the oxide–phenoxide-bridged $Mn^{III}_2Mn^{IV}_2$ species $[Mn_4(O)_4(bpbp)_2](ClO_4)_4$. Although no definitive assignment can be made, **7** still represents the lowest overall oxidation state for a structurally characterised tetranuclear manganese complex with an adamantane core – it is either two or three oxidation levels lower, for example, than $[(tphpn)_2Mn^{III}Mn^{IV}_3(\mu\text{-}O)_4](OTf)_2(ClO_4)_3$.[8] Based on the very small differences of the metric parameters of **7** with the higher oxidation state $Mn_4O_6$ adamantane core compounds in the literature, it can be envisaged that a relatively wide range of oxidation and protonation states may be accessible for $Mn_4O_6$ adamantane core systems without a major structural deformation. A study of the redox chemistry of **7** and its reduced/oxidised and protonated/deprotonated counterparts would be particularly interesting with respect to modelling biological water and oxygen metabolism reactions. This has so far proved impossible in our hands due to solution instability.

## Experimental Section

Elemental analyses were performed at the Chemistry Department II at Copenhagen University, Denmark, and Atlantic Microlab, Inc., Norcross, Georgia 30091, USA. UV/Vis spectra were recorded with a Shimadzu UV-3100 spectrophotometer. ESI mass spectra were obtained using a Finnigan TSQ 700 triple quadrupole instrument equipped with a Finnigan API source in the nanoelectrospray mode. 2,6-Bis{[bis(2-pyridylmethyl)amino]methyl}-4-*tert*-butylphenol (bpbpH),[15] $[tpa_2Mn_2O_2](ClO_4)_3$ [tpa = tris(2-pyridylmethyl)amine],[16] and $[(Me_3tacn)_2Mn_2O_3][PF_6]_2$[7b] were synthesised following literature procedures. $Mn(acac)_2$ and $Mn(acac)_3$ were purchased from Aldrich Chemical company.

***CAUTION!*** *Although no problems were encountered in the preparation of the perchlorate salt, suitable care should be taken when handling such potentially hazardous compounds.*

**$[Mn_2(bpbp)(ClO_4)_2(THF)](ClO_4)\cdot THF\cdot 3H_2O$ ($1\cdot ClO_4\cdot THF\cdot 3H_2O$):** Triethylamine (28.8 μL, 0.21 mmol) was added to a solution of bpbpH (119.2 mg, 0.21 mmol) in degassed THF (3 mL). $Mn(ClO_4)_2\cdot 6H_2O$ (150.1 mg, 0.42 mmol) was then added to give a clear, colourless solution. Air-sensitive white microcrystals of the product deposited over 24 h. Yield: 230.8 mg (92%). $C_{40}H_{47}Cl_3Mn_2N_6O_{14}\cdot C_4H_8O\cdot 3H_2O$: calcd. C 44.85, H 5.22, N 7.13, Cl 9.03; found C 44.89, H 5.16, N 7.15, Cl 9.29. ESI MS ($CH_3CN$): *m*/*z* (%) 390.1 (100) $[(bpbp)Mn_2(ClO_4)]^{2+}$, 879.2 (50) $[(bpbp)Mn_2(ClO_4)_2]^{+}$.

**$[Mn_2(bpbp)(ClO_4)_2(THF)][B(C_6H_5)_4]\cdot 4THF$ ($1\cdot B(C_6H_5)_4\cdot 4THF$):** $1\cdot ClO_4\cdot THF\cdot 3H_2O$ and approx. 4 equiv. of $NaB(C_6H_5)_4$ were dissolved in degassed THF. Slow evaporation under $N_2$ gave very air-sensitive crystals as colourless blocks after a few days.

**$[Mn_2(bpbp)(ClO_4)(H_2O)_2](ClO_4)_2\cdot H_2O$ ($2\cdot (ClO_4)_2\cdot H_2O$):** A solution of $1\cdot ClO_4\cdot THF\cdot 3H_2O$ in degassed $CH_2Cl_2$ (approx. 50 ppm $H_2O$) was allowed to evaporate under $N_2$. Air-sensitive crystals formed as colourless blocks overnight.

**$[Mn_2(bpbp)(OCH_3)_2(H_2O)_2](ClO_4)_2$ ($3\cdot (ClO_4)_2$):** Triethylamine (113 mg, 1.11 mmol) was added to a pale-green solution of $Mn(ClO_4)_2\cdot 6H_2O$ (862 mg, 2.38 mmol) and bpbpH (599 mg, 1.05 mmol) in methanol (14 mL). The initially colourless solution changed to red brown. Dark-purple crystals of the product deposited over 24 h. Yield: 320 mg (31%). $C_{38}H_{49}Cl_2Mn_2N_6O_{13}$: calcd. C 46.64, H 5.05, N 8.59, Cl 7.25; found C 45.79, H 5.10, N 8.68, Cl 7.36. ESI MS (mild source conditions, $CH_3OH$): *m*/*z* (%) 348.8 (100) $[(bpbp)Mn_2O]^{2+}$, 357.7 (50) $[(bpbp)Mn_2(OH)_2]^{2+}$, 366.8 (30) $[(bpbp)Mn_2(OH)_2(H_2O)]^{2+}$, 371.8 (5) $[(bpbp)Mn_2(OCH_3)_2]^{2+}$, 375.7 (20) $(bpbp)Mn_2(OH)_2(H_2O)_2]^{2+}$. UV/Vis ($CH_3OH$): $\lambda_{max}$, ($\varepsilon$) = 309 nm (17200 L mol$^{-1}$ cm$^{-1}$), 258 (4560).

Alternatively, recrystallisation of $1\cdot ClO_4\cdot THF\cdot 3H_2O$ from dry MeOH in air gave $3\cdot (ClO_4)_2$.

**$[Mn_4(O)_2(OH)_2(bpbp)_2](ClO_4)_4$ ($7\cdot (ClO_4)_4$):** A solution of $1\cdot ClO_4\cdot THF\cdot 3H_2O$ (25 mg, 0.021 mmol) in dry THF (50 mL) was treated with 2 equiv. of *tert*-butylhydrogen peroxide (6 M in decane). The solution turned black. The mixture was allowed to stand in an open flask until dryness and the very small brown crystals used for the structural analysis were recovered. All other preparations of this material resulted in dark amorphous powders which give no XRPD pattern. Thus, the homogeneity of the bulk sample of this compound is not clear despite the fact that elemental analyses are consistent with the proposed formulation. $C_{72}H_{80}Cl_4Mn_4N_{12}O_{22}$: calcd. C 47.33, H 4.41, N 9.2, Cl 7.76; found (average) C 46.99, H 4.36, N 9.15, Cl 7.50.

**X-ray Crystallography:** Analysis of $1\cdot B(C_6H_5)_4\cdot 4THF$ was done at 180(2) K on a Bruker Nonius X8-APEXII instrument at the University of Southern Denmark. The structure was solved by direct methods and refined against all $F^2$ data using software incorporated in WinGX ver. 1.70.[17] The geometry of all solvent THF molecules was restrained and each THF molecule was refined with one isotropic displacement parameter. The O-position of one solvent THF could not be determined. Two of the remaining solvent THF molecules as well as the coordinated THF and the perchlorates were all refined with isotropic displacement parameters as disordered over two positions with equal occupancy, except for the position of the non-bridging perchlorate, which was refined with 33/66% occupancy. The chloride in the bridging perchlorate as well as all remaining non-hydrogen atoms were refined with anisotropic atomic displacement parameters, and hydrogen atoms bonded to carbon were inserted at calculated positions using a riding model. Crystals of $7\cdot (ClO_4)_4$ were too weakly diffracting for data collection using a standard laboratory sealed-tube source and so the data were collected at 150 K at Station 9.8 of the Synchrotron Radiation Source at Daresbury.[18] The structure was solved by direct methods and refined by full-matrix least-squares on $F^2$ using the SHELXTL package.[19] The cation has a twofold axis passing through the two phenolic oxygen atoms, there is disorder of the two *tert*-butyl groups and in one of the perchlorate anions these were both modelled with equal occupancy of two positions. All non-hydrogen atoms were refined with anisotropic atomic displacement parameters and hydrogen atoms bonded to carbon were inserted at calculated positions using a riding model; hydrogen atoms bonded to oxygen were not located and were not included in the model. Since the crystals were formed by complete evaporation of a reaction mixture, the high *R*-value might be ascribed to crystal defects caused by solvent loss. Voids remain in the structure ($4\times 204$ Å$^3$ per unit cell) but because of the weak diffraction data SQUEEZE[20] could not be used to estimate the electron density and it can therefore not be excluded that diffuse solvent molecules are located in these voids. Data collection and structure refinement details are summarised in Table 4.

  

CCDC-613204 (for **1·ClO$_4$·THF·3H$_2$O**) and -613205 [for **7·(ClO$_4$)$_4$**] contain the supplementary crystallographic data for this paper. These data can be obtained free of charge from The Cambridge Crystallographic Data Centre via www.ccdc.cam.ac.uk/data_request/cif.

Table 4. Crystallographic details.

| | **1**·B(C$_6$H$_5$)$_4$·4THF | **7**·(ClO$_4$)$_4$ |
|---|---|---|
| Empirical formula | $C_{80}H_{99}BCl_2Mn_2N_6O_{14}$ | $C_{72}H_{80}Cl_4Mn_4N_{12}O_{22}$ |
| $M_r$ | 1560.24 | 1827.04 |
| $\lambda$ [Å] | 0.71073 | 0.69410 |
| Crystal system | triclinic | monoclinic |
| Space group | $P\bar{1}$ | $C2/c$ |
| $Z$ | 2 | 4 |
| $a$ [Å] | 13.346(2) | 16.427(4) |
| $b$ [Å] | 14.490(3) | 24.404(4) |
| $c$ [Å] | 21.206(4) | 20.902(4) |
| $\alpha$ [°] | 78.589(7) | 90 |
| $\beta$ [°] | 86.275(7) | 93.402(6) |
| $\gamma$ [°] | 79.374(7) | 90 |
| $U$ [Å$^3$] | 3949.2(12) | 8365(3) |
| Crystal size [mm] | 0.40 × 0.16 × 0.08 | 0.20 × 0.10 × 0.02 |
| Crystal colour | colourless | brown |
| $T$ [K] | 180(2) | 150(2) |
| $\rho_{calcd.}$ [g cm$^{-3}$] | 1.312 | 1.451 |
| $\mu$(Mo-$K_\alpha$) [mm$^{-1}$] | 0.454 | 0.795 |
| $F$(000) | 1644 | 3760 |
| $T_{min}$, $T_{max}$ | 0.8394, 0.9646 | |
| $\theta_{min}$, $\theta_{max}$ [°] | 3.52 to 21.96 | 2.34 to 25.00 |
| Completeness to $\theta_{max}$ | 0.988 | 0.995 |
| Data collected | 33507 | 30596 |
| Unique data | 9530 | 7868 |
| $R_{int}$ | 0.0953 | 0.1404 |
| Observed data [$I > 2\sigma(I)$] | 5547 | 6145 |
| Parameters, restraints | 834, 92 | 590, 727 |
| Goof, $S$ | 1.037 | 1.236 |
| $R_1$, $wR_2$ [$I > 2\sigma(I)$] | 0.0907, 0.2447 | 0.2156, 0.4303 |
| $R_1$, $wR_2$ [all data] | 0.1552, 0.2957 | 0.2424, 0.4415 |
| $\rho_{min}$, $\rho_{max}$ [e Å$^{-3}$] | 0.755, –0.673 | 1.480, –1.712 |

**Magnetochemistry:** A Quantum Design MPMS5 Squid magnetometer was used to obtain magnetic susceptibility in a field of 1 T. Samples with a mass of about 20 mg were contained in a calibrated gelatine capsule which was held in the centre of a plastic drinking straw fixed to the sample oval. The instrument was calibrated by use of a standard palladium sample supplied by Quantum Design Inc. Magnetisation isotherms (2–20 K and 0–5 T fields) were obtained on a sample of **7**·(ClO$_4$)$_4$ dispersed in a Vaseline mull in order to prevent torquing of crystallites and production of anomalous data.

**XANES:** Complexes were diluted with boron nitride and data were obtained in fluorescence mode on beamlines X9B or X18 of the National Synchrotron Light Source, using the inflection point of a Mn foil spectrum at 6539.0 eV as the energy calibration. The general procedures for obtaining XANES spectra (which are normalised to the edge height) from the fluorescence data were similar to those used previously for iron and cobalt compounds.[10,21]

**Supporting Information** (see footnote on the first page of this article): Isothermal magnetisation data for **7**·(ClO$_4$)$_4$.

## Acknowledgments

Support from the Danish Technical and Natural Science Research Council (grant, 26-02-0192), DANSYNC and COST project no. D21/0010/01 is gratefully acknowledged. V.M. is grateful to the EPSRC for access to Station 9.8 of the SRS at Daresbury. X-ray beam time for the EXAFS and XANES study was provided at beam lines X9B and X18B through the General Users Program of the National Synchrotron Light Source, which is supported by the US Department of Energy, Divisions of Materials Science and Chemical Science (DOE contract number DE-AC02-76CH00016). K.S.M. thanks the Australian Research Council for support for the magnetic studies.

[1] a) R. Hage, J. Kerschner, *Trends Inorg. Chem.* **1998**, *5*, 145–159; b) K. F. Sibbons, K. Shastri, M. Watkinson, *Dalton Trans.* **2005**, 645–661.
[2] K. B. Jensen, E. Johansen, F. B. Larsen, C. J. McKenzie, *Inorg. Chem.* **2004**, *43*, 3801–3803.
[3] F. H. Allen, *Acta Crystallogr. Sect. B* **2002**, *58*, 380–388.
[4] S. Brooker, V. McKee, T. Metcalfe, *Inorg. Chim. Acta* **1996**, *246*, 171–179.
[5] A. Boisen, A. Hazell, C. J. McKenzie, *Chem. Commun.* **2001**, 2136–2137.
[6] M. Ghiladi, F. B. Larsen, C. J. McKenzie, I. Søtofte, J.-P. Tuchagues, *Dalton Trans.* **2005**, 1687–1692.
[7] a) K. Wieghardt, U. Bossek, W. Gebert, *Angew. Chem. Int. Ed. Engl.* **1983**, *22*, 328–329; b) K. Wieghardt, U. Bossek, B. Nuber, J. Weiss, J. Bonvoisin, M. Corbella, S. E. Vitols, J. J. Girerd, *J. Am. Chem. Soc.* **1988**, *110*, 7398–7411; c) C. E. Dubé, D. W. Wright, W. H. Armstrong, *J. Am. Chem. Soc.* **1996**, *118*, 10910–10911; d) K. S. Hagen, T. D. Westmoreland, M. J. Scott, W. H. Armstrong, *J. Am. Chem. Soc.* **1989**, *111*, 1907–1909; e) C. E. Dube, D. W. Wright, S. Pal, P. J. Bonitatebus Jr, W. H. Armstrong, *J. Am. Chem. Soc.* **1998**, *120*, 3704–3716; f) C. E. Dubé, S. Mukhopadhyay, P. J. Bonitatebus Jr, R. J. Staples, W. H. Armstrong, *Inorg. Chem.* **2005**, *44*, 5161–5175.
[8] S. Mukhopadhyay, H. J. Mok, R. J. Staples, W. H. Armstrong, *J. Am. Chem. Soc.* **2004**, *126*, 9202–9204.
[9] I. D. Brown, D. Altermatt, *Acta Crystallogr. Sect. B* **1985**, *41*, 244–247.
[10] R. C. Scarrow, B. A. Brennan, J. G. Cummings, H. Jin, D. J. Duong, J. Kindt, M. J. Nelson, *Biochemistry* **1996**, *35*, 10078–10088.
[11] a) D. M. Eichhorn, W. A. Armstrong, *J. Chem. Soc., Chem. Commun.* **1992**, 85–87; b) Z. Shirin, V. G. Young Jr, A. S. Borovik, *Chem. Commun.* **1997**, 1967–1968; c) S. Pal, M. K. Chan, W. H. Armstrong, *J. Am. Chem. Soc.* **1992**, *114*, 6398–6406; d) T.-S. Lai, H.-L. Kwong, C.-M. Che, S.-M. Peng, *Chem. Commun.* **1997**, 2373–2374; e) Z. Shirin, B. S. Hammes, V. G. Young Jr, A. S. Borovik, *J. Am. Chem. Soc.* **2000**, *122*, 1836–1837; f) S. Pal, W. H. Armstrong, *Inorg. Chem.* **1992**, *31*, 5417–5423; g) T. J. Hubin, J. M. McCormick, N. W. Alcock, D. H. Busch, *Inorg. Chem.* **2001**, *40*, 435–444; h) M. Corbella, R. Costa, J. Ribas, P. H. Fries, J.-M. Latour, L. Öhrstrom, X. Solans, V. Rodriguez, *Inorg. Chem.* **1996**, *35*, 1857–1865.
[12] a) P. Dalgaard, C. J. McKenzie, *J. Mass Spectrom.* **1999**, *34*, 1033–1039; b) Y. Dussart, C. Harding, P. Dalgaard, C. McKenzie, R. Kadirvelraj, V. McKee, J. Nelson, *J. Chem. Soc., Dalton Trans.* **2002**, 1704–1713.
[13] L. Dubois, D.-F. Xiang, X.-S. Tan, J. Pécaut, P. Jones, S. Baudron, L. Le Pape, J.-M. Latour, C. Baffert, S. Chardon-Noblat, M.-N. Collomb, A. Deronzier, *Inorg. Chem.* **2003**, *42*, 750–760 and references cited therein for $J$ values for related $Mn^{II}Mn^{III}$ complexes. The $J$ value is similar to that of related bis-carboxylate-bridged $Mn^{II}$–$Mn^{III}$ systems.
[14] K. S. Murray, *Adv. Inorg. Chem.* **1995**, *43*, 261–358.
[15] M. Ghiladi, C. J. McKenzie, A. Meier, A. K. Powell, J. Ulstrup, S. Wocaldo, *J. Chem. Soc., Dalton Trans.* **1997**, 4011–4018.
[16] D. K. Towle, C. A. Botsford, D. J. Hodgson, *Inorg. Chim. Acta* **1988**, *141*, 167–168.
[17] L. J. Farrugia, *J. Appl. Crystallogr.* **1999**, *32*, 837–838.

  

[18] R. J. Cernik, W. Clegg, C. R. A. Catlow, G. Bushnell-Wye, J. V. Flaherty, G. N. Greaves, M. Hamichi, I. Burrows, D. J. Taylor, S. J. Teat, *J. Synchrotron Radiat.* **1997**, *4*, 279–286.
[19] G. M. Sheldrick, SHELXTL version 5.1, Bruker AXS, Madison, Wisconsin, USA **1997**.
[20] A. L. Spek, *J. Appl. Crystallogr.* **2003**, *36*, 7–13.
[21] K. M. Padden, J. F. Krebs, K. T. Trafford, G. P. Yap, A. H. Rheingold, A. S. Borovik, R. C. Scarrow, *Chem. Mater.* **2001**, *13*, 4305–4313.

Received: May 25, 2006
Published Online: August 7, 2006

  